Published in final edited form as:
Mol Pharm. 2008 ; 5(4): 527–539. doi:10.1021/mp800022a.

Synthesis, Characterization, and Biological Evaluation of Integrin $\alpha_v\beta_3$-Targeted PAMAM Dendrimers

C. Andrew Boswell[†,¥], **Peter K. Eck**[‡], **Celeste A. S. Regino**[‡], **Marcelino Bernardo**[§,‡], **Karen J. Wong**[‡], **Diane E. Milenic**[†], **Peter L. Choyke**[‡], and **Martin W. Brechbiel**[*,†]

†*Radioimmune & Inorganic Chemistry Section, Radiation Oncology Branch, National Cancer Institute, National Institutes of Health, Bethesda, 20892-1088*

‡*Molecular Imaging Program, Center for Cancer Research, National Cancer Institute, National Institutes of Health, Bethesda, Maryland 20892-1088*

§*Imaging Physics, Laboratory Animal Sciences Program, SAIC-Frederick, Inc., NCI-Frederick, Frederick, MD 21702*

Abstract

Ligand size and valency strongly influence the receptor uptake and clearance of tumor angiogenesis imaging agents. The structures of successful imaging agents exhibit a high degree of variability, encompassing small mono-valent arginine-glycine-aspartic acid (RGD)-containing peptides, multivalent RGD-oligomers, and a monoclonal antibody against integrin *alpha*-v-*beta*-3 ($\alpha_v\beta_3$). We have pursued a nano-scale approach to imaging of angiogenesis using rationally designed polyamidoamine (PAMAM) dendrimers covalently adorned with RGD-cyclopeptides. An orthogonal oxime-ligation strategy was applied to chemoselectively effect conjugation of the PAMAM dendrimers with RGD-cyclopeptides for targeting $\alpha_v\beta_3$. Fluorescent dyes for optical imaging and chelates for gadolinium-based magnetic resonance (MR) imaging were subsequently appended to create robust multimodal macromolecular imaging agents. Fluorescence microscopy revealed selective binding of the resulting RGD peptide-bearing dendrimer with empty chelates to $\alpha_v\beta_3$-expressing cells, but somewhat reduced selectivity was observed following Gd(III) complexation. The expected incomplete saturation of chelates with Gd(III) ions permitted radiometal complexation, and an *in vivo* tissue distribution of the resulting agent in M21 melanoma tumor-bearing mice showed mostly renal and reticuloendothelial accumulation, with the tumor:blood ratio peaking (3.30 ± .03) at 2 hr post-injection.

Keywords

Dendrimer; angiogenesis; $\alpha_v\beta_3$; RGD peptide; multimodal imaging; optical imaging; optical microscopy; flow cytometry; γ-scintigraphic imaging; MRI

INTRODUCTION

Polyamidoamine (PAMAM) dendrimers have received considerable attention since their introduction by Tomalia and co-workers in 1985.[1,2] Key to their success is an availability of a variety of sizes, termed "generations", that allows for fine-tuning molecular size to match a

*Correspondence to: Martin W. Brechbiel, Ph.D., Radioimmune & Inorganic Chemistry Section, Radiation Oncology Branch, NCI, NIH, Building 10, Room 1B40, 10 Center Drive, Bethesda, MD 20892-1088, Fax: (301) 402-1923.
¥Current address: Genentech, Inc., 1 DNA Way, MS 70, South San Francisco, CA 94080 Email: martinwb@mail.nih.gov

given application. Extensive studies have revealed many intrinsic properties deemed ideal for use in biomedical applications.[1–3] Application as a novel drug platform was confirmed when PAMAM dendrimers bearing chelated gadolinium (Gd(III)) emerged as a novel class of magnetic resonance imaging (MRI) contrast agents featuring high molar relaxivities and superb image enhancement.[4,5] By combining these properties with the advanced imaging capabilities of dynamic contrast-enhanced MRI (DCE-MRI), a clearer picture of uptake, washout kinetics, vascularization, and permeability in tumors and other tissues may became possible.[6,7]

The MRI contrast agent properties of these Gd(III)-loaded dendrimers (i.e. gadomers) have been further explored alone,[8–10] conjugated to avidin/biotin,[11] conjugated to monoclonal antibodies,[12] or targeted to high-affinity folate receptors.[13] Shukla and co-workers evaluated a non-MRI-based, fluorescently labeled generation 5 PAMAM dendrimer modified with doubly-cyclized RGD peptides containing two disulfide linkages via four cysteine residues.[14] Langereis and co-workers reported the synthesis of a Gd(III)-DTPA-functionalized dendritic contrast agent modified with a cyclic NGR sequence to encourage preferential binding to tumor vasculature.[15]

Multimodal molecular imaging agents are desirable because of the synergy generated from overlapping the strengths of each individual modality thereby compensating for individual inherent limitations. Because of their numerous available conjugation sites, dendrimers are excellent platforms combining MRI, optical, PET, CT and γ-scintigraphic imaging capabilities into a single macromolecular entity. Recent efforts towards multimodal imaging agents include a dendrimeric multimodal imaging agent that combined aspects of MRI and optical imaging.[16] This specific article details efforts extending those prior results towards an application of imaging tumor angiogenesis.

Vascular $\alpha_v\beta_3$ integrin regulates the production of vascular endothelial growth factor (VEGF) in tumor cells required for tumor angiogenesis through activation, clustering, and signaling.[17] Consequently, development of radiolabeled integrin $\alpha_v\beta_3$ antagonists for molecular imaging and therapy of tumors is a burgeoning effort.[18] Human endothelial cells express integrin receptors on both the apical (luminal) and basal-lateral (substratum-attached) aspects of their membranes which suggests the apical membrane is exposed and accessible to a putative circulating radiopharmaceutical.[19] The distinction should be drawn, however, that the vast majority of literature imaging studies detail delineation of tumors in which $\alpha_v\beta_3$ receptors are expressed on both the vasculature endothelium surrounding the tumor *and on the tumor cells themselves*.[20]

Multivalent RGD-containing agents have shown greater overall success compared to monovalent RGD agents.[21,22] However, it is unresolved whether the observed superior results of multivalent ligand constructs are truly due to polyvalent interactions[22] or merely a size effect (i.e., enhanced permeability and retention (EPR)).[23,24] Use of dendrimers as a platform for RGD-cyclopeptides provides a unique opportunity wherein agents of varying sizes (generations) and degrees of modification are possible. Besides dendrimers, other macromolecular strategies include water-soluble co-polymers,[25] contrast-enhanced ultrasound with microbubbles,[26] and a humanized monoclonal antibody.[27]

The requirement of aspartic acid (D) for RGD-integrin binding[28] is a key consideration in the design of these peptide component imaging agents. This side chain necessitates use of chemistry orthogonal to the carboxylic acid functional group. Oxime ligation has been successfully used *in vivo* attesting to the stability of the resulting covalent linkage.[29] In the presence of periodate, *N*-terminal serine and threonine residues are oxidized to an aldehyde or ketone, respectively,[30] with which an aminooxy group selectively reacts at mildly acidic conditions (pH ~5).

Herein are described the synthesis, characterization, and biological evaluation of PAMAM dendrimers with chemoselectively-ligated RGD-cyclopeptides (Figure 1, X=H) or control RAD-cyclopeptides (Figure 1, X=CH_3) for multimodal imaging of tumor angiogenesis. These complex macromolecular constructs were synthesized in a rational, step-wise manner exploiting orthogonal aminooxy/aldehyde chemistry for peptide conjugation combined with standard succinimidyl ester and isothiocyanate chemistry for dye and chelate conjugation, respectively (Figure 2) to provide the final targeted multi-modality dendrimer-based imaging agents. The abilities of the resulting dendrimer-based agents to bind cultured $\alpha_v\beta_3$-expressing M21 cells were evaluated by fluorescence microscopy, and the *in vivo* tissue distribution of the ^{111}In-labeled RGD-bearing dendrimer was assessed in M21 tumor-bearing mice. Encouraging results were obtained *in vitro*; excellent binding selectivity to the integrin-expressing cells was observed prior to complexation of Gd(III) by the pendant chelates, and the detection of partial nonspecific binding of the corresponding Gd(III)-containing agents was attributed to a reduction in their hydrophilic natures upon metal loading. The RGD peptide-bearing gadomer was also labeled with ^{111}In using available empty chelates, and an *in vivo* tissue distribution study in tumor-bearing mice showed disappointingly little tumor accumulation; the highest measured uptake was 1.25 ± 0.51 % injected dose per gram at 2 hours post-injection. Because detection of gadolinium-based contrast agents is far less sensitive than radionuclide detection, *in vivo* MR imaging was not pursued.

EXPERIMENTAL METHODS

Materials

The peptides c(RGDfK), c(RADfK), c(RGDfK(S)), and (RADfK(S)) were obtained from Peptides International, Inc. (Louisville, KY). Generation 3 PAMAM ethylenediamine core dendrimer was obtained from Dendritech®, Inc (Midland, MI) as a 20% w/v in methanol. The bifunctional chelating agents, 2-(4-isothiocyanatobenzyl)-6-methyl-diethylenetriaminepentaacetic acid (1B4M-DTPA)[31] and *N*-[(*R*)-2-amino-3-(*p*-5-[(2,5-dioxopyrrolidin-1-yl)oxy]-5-oxo-*N*-phenylpentanamide) propyl]-*trans*-(*S*,*S*)-cyclohexane-1,2-diamine- *N*,*N*,*N*′,*N*″,*N*#-penta-*tert*-butyl acetate (CHX-A”-NHS)[32] were prepared as previously described. The *N*-hydroxysuccinimidyl ester of *N*-(*tert*-butoxycarbonyl)-*O*- (carboxymethyl)hydroxylamine (**1**) was prepared as previously described.[33] All other reagents were purchased from Aldrich (St. Louis, MO) and were used as received. Purified integrin $\alpha_v\beta_3$ was obtained from Chemicon International, Inc. (Temecula, CA). Centriprep® centrifugal filter units with Ultracel-YM10 regenerated cellulose membranes (10,000 kDa Nominal Molecular Weight Limit) were purchased from Millipore Corp. (Billerica, MA). Reversed-phase Sep-Pak® solid-phase extraction (SPE) cartridges were purchased from Waters Corp. (Milford, MA).

Chemistry

Characterizations and structural confirmations of dendrimer-based intermediates and products were performed by ^{1}H NMR, size-exclusion HPLC, and MALDI-TOF mass spectrometry. Characterization of low-MW intermediates was performed by ^{1}H NMR, electrospray mass spectrometry, and reversed phase HPLC. ^{1}H and ^{13}C NMR data were obtained using a Varian Gemini 300 MHz instrument and chemical shifts are reported in ppm on the δ scale relative to TMS, TSP or solvent. Proton chemical shifts are annotated as follows: ppm (multiplicity, integration). Elemental analyses were performed by Desert Analytics (Tucson, AZ) using combustion analysis method for C, H, N, and S, and inductively coupled plasma-atomic emission spectroscopy (ICP-AES) method for determining the percentage of Gd. MALDI-TOF analysis of modified dendrimers was performed by The Scripps Center for Mass Spectrometry (La Jolla, CA). Electrospray mass spectra using an electrospray ionization mode (ESI/TOF/MS) were obtained using Waters LCT Premier Time of Flight Mass Spectrometer operated in

positive or negative ion mode. The electrospray capillary voltage was 3kV and the sample cone voltage was 60V. The desolvation temperature was 225 °C, and the desolvation gas flow rate was nitrogen at 300 L/hr. Accurate masses were obtained using the lock spray mode with Leu-Enkephalin as the external reference compound.

Dendrimer conjugation and purity was assessed by size exclusion HPLC (SE-HPLC) using a Beckman System Gold (Fullerton, CA) equipped with model 126 solvent delivery module and a model 168 UV detector (λ 254 and 280 nm) controlled by 32 Karat software. Size exclusion chromatography was performed on a Tosohaas G3000SW, 10 μm, 7.8 mm × 30 cm column (Montgomeryville, PA) using phosphate buffered saline (1X PBS) solution as the eluent (0.5 mL/min). Semi-preparative reversed phase HPLC was performed using two Gilson Model 303 pumps, a Gilson 803C manometric module, a Gilson 811B dynamic mixer, and a Knauer ultraviolet detector all connected through a Gilson 506C system interface module and operated by UniPoint version 1.65 software. Purification of peptide-dye conjugates was achieved with a Hamilton Prp-1 polymer reversed phase semi-preparative column (10 μm, 7.0 mm × 30.5 cm) using a flow rate of 3 mL/min and a gradient of 100% A to 50% B over a 20-min time period where A = 15 mM NH_4OAc pH 7.0 and B = CH_3CN.

Synthesis of peptide-chelate conjugate

Direct conjugation of CHX-A’’-NHS to the c(RGDfK) peptide was performed as previously described.[32] Briefly, c(RGDfK) (100 mg) was suspended in DMF (1 mL) and the CHX-A”-NHS ester (1.5 eq) was added in one portion. The suspension cleared after 10 – 30 min. The reaction was allowed to proceed for ~8 hr, and the crude product was isolated by precipitation with Et_2O. The *tert*-butyl ester groups were cleaved using TFA, and the crude product was purified by reversed-phase C_{18} chromatography using aqueous TFA (1%) with an increasing CH_3CN gradient in the mobile phase. High resolution ESI/TOF/MS calculated for *tert*-butyl protected CHX-A”- c(RGDfK) conjugate $[C_{84}H_{119}N_{13}O_{14}]^+$: 1533.8999, found: 1533.9020. ESI/TOF/MS calculated for the deprotected CHX-A”-c(RGDfK) conjugate $[C_{57}H_{81}N_{13}NaO_{19}]^+$: 1274.7, found: 1276.3.

Synthesis of peptide-dye conjugates

Direct conjugation of Alexa Fluor 594 carboxylic acid, succinimidyl ester (mixed isomers) (Invitrogen Corporation, Carlsbad, CA) to both c(RGDfK) and c(RADfK) peptides was performed using a standard conjugation approach. To Alexa Fluor 594 NHS ester (2.0 mg) in DMF (750 μL) was added c(RGDfK) (1.5 mg) or c(RADfK) (1.5 mg). A single drop of diisopropylethylamine was added to the reaction mixture to serve as a catalytic base. Both reactions were constantly stirred in the dark under argon for 12 hr. The crude reaction mixtures were each subjected to semi-preparative HPLC purification as described above. Relevant peaks were collected, lyophilized, and analyzed by mass spectrometry for characterization. The quantum yield was determined relative to the original dye. Because Alexa Fluor 594 NHS exists as a mixture of structural isomers, two isomeric products were anticipated and were indeed observed. The isomers were isolated and characterized by mass spectrometry separately; however, assigning each peak to its corresponding structure was not pursued as substitution at the 5- versus 6-position of the aromatic ring in the fluorophore is not expected to significantly influence the integrin-binding ability of each cyclic peptide. As such, we selected the major isomeric product (the later peak fraction) of both the c(RGDfK)- and c(RADfK)-conjugated peptides for biological evaluation by confocal microscopy. ESI/TOF/MS calculated for c(RGfDK)-Alexa Fluor 594 $[C_{62}H_{72}N_{11}O_{17}S_2]^-$: 1306.46, found: 1306.4. ESI/TOF/MS calculated for c(RAfDK)-Alexa Fluor 594 $[C_{63}H_{74}N_{11}O_{17}S_2]^-$: 1320.48, found: 1320.4. Relative quantum yield for c(RGfDK)-Alexa Fluor 594: 0.73 ± 0.13. Relative quantum yield for c(RAfDK)-Alexa Fluor 594: 0.70 ± 0.10.

Aminooxy functionalization of dendrimer(2)

The step-wise modification of the dendrimers is outlined in Figure 1. The terminal amines of G3 PAMAM dendrimers were reacted with **1** using a 1:2 molar ratio in bicarbonate buffer. In brief, **1** (56 mg, 2 eq) was added to dry PAMAM generation 3 dendrimer (G3) (667 mg) in bicarbonate buffer (20 mL) (pH 8.5; 0.002 M Na_2CO_3, 0.048 M $NaHCO_3$, 0.15 M NaCl). Following incubation at 25 °C for 18 hr under argon with constant stirring, the reaction mixture was subjected to exhaustive membrane dialysis against H_2O using Amicon® stirred ultrafiltration cells with YM3 cellulose membranes (Millipore Corp., Billerica, MA) having a 3,000 Da molecular weight cutoff. The resulting *tert*-butyl-protected aminooxy-functionalized dendrimer crude product (**2**) was isolated by lyophilization to give 649 mg of a light yellow solid. ^{1}H-NMR was used to estimate the average number of aminooxy moieties per dendrimer macromolecule through comparative peak integration of the unique *tert*-butyl protons versus the core dendrimer protons.

The crude protected aminooxy-pendant dendrimer **2** (333 mg) was reacted with neat trifluoroacetic acid (TFA) (30 mL) for 18 hr at 25°C under argon with constant stirring to fully deprotect the *tert*-butyl esters. Excess TFA was removed by rotary evaporation, with residual TFA being removed by repeated co-evaporation with CH_2Cl_2. The resulting residue was transferred into water and subjected to an exhaustive membrane dialysis against H_2O using Amicon® stirred ultrafiltration cells with YM3 cellulose membranes (Millipore Corp., Billerica, MA) having a 3,000 Da molecular weight cutoff. A very hygroscopic yellow solid **3** (326 mg) was isolated. The resulting aminooxy-functionalized dendrimer product (**3**) was characterized by ^{1}H-NMR. Elemental analysis calculated for $[(C_{302}H_{608}N_{122}O_{60})(C_2H_5NO_2)_2(C_2HF_3O_3)_{54}(H_2O)_5]$: C, 37.34; H, 5.16; N, 13.05. Found: C, 37.61; H, 4.59; N, 12.51.

Oxime-ligation of c(RXDfK)-peptide aldehyde to aminooxy-modified dendrimers (4a and 4b)

Peptide aldehydes, c(RGDfK)- or c(RADfK)-peptide aldehyde, were prepared as previously described using the periodate-driven oxidation protocol of c(RGDfK(S)).[30,34] In brief, $NaIO_4$ (83 mg, 0.388 mmol)) in PBS (pH 7.0) was added to c(RGDfK(S)) (89 mg, 0.129 mmol) (Peptides International, Louisville, KY). In parallel, $NaIO_4$ (76.5 mg, 0.358 mmol) in PBS (pH 7.0) was added to c(RADfK(S)) (84 mg, 0.119 mmol). Following a 5 min incubation with manual shaking at 25°C, the peptide aldehydes were promptly separated from excess periodate and buffer salts using C-18 Sep-Pak cartridges to prevent over-oxidation to their respective undesired carboxylic acids. The isolated aldehydes were lyophilized to yield fluffy white solids (46.9 mg of the c(RGDfK) peptide aldehyde and 46.6 mg of the c(RADfK) peptide aldehyde) and were characterized by electrospray mass spectrometry and analytical reversed-phase HPLC prior to coupling to the dendrimer. High resolution ESI/TOF/MS calculated for c(RADfK) aldehyde $[C_{30}H_{44}N_9O_9]^+$: 674.3262; found, 674.3258. High resolution ESI/TOF/MS calculated for c(RGDfK) aldehyde $[C_{29}H_{42}N_9O_9]^+$: 660.3105; found, 660.3123.

A 1:1 molar ratio of the c(RGDfK)- or c(RADfK)-peptide aldehyde (aminooxy number basis) was site-specifically reacted with the aminooxy residues of **3** to yield **4a** and **4b**, respectively. In brief, c(RGDfK(S)-peptide aldehyde (30.4 mg, 0.044 mmol, 2 eq) was added to of **3** (162.5 mg, 1 eq) in NaOAc buffer (pH 4.8). Likewise, c(RADfK(S)-peptide aldehyde (31.0 mg, 0.044 mmol, 2 eq) was added to **3** (162.5 mg, 1 eq) in NaOAc buffer (pH 4.8). The reaction mixtures were allowed to stir under argon for 18 hr, and were subjected to exhaustive membrane dialysis against H_2O using 3,000 Da molecular weight cutoff Amicon® membranes (Millipore Corp., Billerica, MA). The purified dendrimer-peptide conjugates (**4**) were lyophilized to yield yellow hygroscopic solids (142 mg of **4a**; 145 mg of **4b**). Peptide-dendrimer conjugation was confirmed by ^{1}H-NMR spectroscopy in D_2O. The peptide-dendrimer conjugates were also characterized by elemental analysis. Elemental analysis calculated for **4a**:

$[(C_{302}H_{608}N_{122}O_{60})(C_2H_5NO_2)_2(C_{30}H_{45}N_9O_8)_{2.6}(C_2H_4O_2)_{65}Na_{72}(H_2O)_9]$: C, 42.24; H, 6.99; N, 14.21. Found: C, 42.16; H, 5.64; N, 13.99. Elemental analysis calculated for **4b**: $[(C_{302}H_{608}N_{122}O_{60})(C_2H_5NO_2)_2(C_{30}H_{45}N_9O_8)_{1.5}(C_2H_4O_2)_{35}Na_{42}(H_2O)_{27}]$: C, 43.39; H, 7.61; N, 16.54. Found: C, 43.41; H, 6.98; N, 16.84.

Sequential conjugation of Alexa Fluor 594 and 1B4M-DTPA to c(RXDfK)-modified dendrimers (6)

The peptide-modified G3 dendrimers (**4**) were reacted with one molar equivalent of the activated optical dye, Alexa Fluor 594 carboxylic acid, succinimidyl ester (mixed isomers) (Invitrogen Corp., Carlsbad, CA) followed 8 hr later by a 2-fold molar excess (surface primary amine number basis) of 1B4M-DTPA. Briefly, Alexa Fluor 594 carboxylic acid, succinimidyl ester (mixed isomers) (3.5 mg, 4.28 μmol, 1 eq) was added to **4a** (40 mg, 1 eq) or **4b** (40 mg, 1 eq) in bicarbonate buffer (pH 8.5, 0.002 M Na_2CO_3, 0.048 M $NaHCO_3$, 0.15 M NaCl). The light-sensitive dye moiety was protected from light during this and all subsequent reaction and purification steps. The reactions were stirred in darkness under argon for 12 hr, at which point the 1B4M-DTPA (0.103 g, 0.186 mmol, 1 eq on a surface primary amine number basis) was added to each mixture. After 24 hr of reaction with constant stirring in darkness at 25°C under argon, additional 1B4M DTPA (0.103 g, 0.186 mmol, 1 eq) was added (for a total of 2:1, 1B4M:amine molar excess). This reagent was added in two aliquots (24 hr apart) to maximize the number of 1B4M-DTPA units covalently attached to the dendrimer molecules via thiourea linkages. After an additional 24 hr in darkness at 25°C under argon with constant stirring, the reaction mixtures were subjected to an exhaustive membrane dialysis against deionized H_2O using 3,000 Da molecular weight cutoff Amicon® membranes (Millipore Corp., Billerica, MA). The purified peptide-dendrimer-dye conjugates (**6**) were lyophilized and characterized by elemental analysis and size-exclusion chromatography. The quantum yield was determined relative to the original dye. Lyophilization of the retentates provided the products as fluffy light purple hygroscopic solids: 0.118 g of **6a** and 0.111 g of **6b**. The number of 1B4M-DTPA units per dendrimer molecule was established by elemental analysis. Elemental analyis calculated for **6a** $[(C_{302}H_{608}N_{122}O_{60})(C_2H_5NO_2)_2(C_{29}H_{43}N_9O_8)_2(C_{23}H_{30}N_4O_{10}S)_{27}(C_{37}H_{34}N_2O_{10}S_2)_{0.75}Na_{63}(H_2O)_{95}]$: C, 44.90; H, 6.44; N, 13.02; S, 3.38. Found: C, 45.36; H, 6.71; N, 12.45; S, 2.78. MALDI-TOF expected for $[\mathbf{6a}\cdot Na_{26}(H_2O)_{565}]^{2+}$: 18 683; Found: m/z = 18 681. Elemental analyis calculated for **6b** $[(C_{302}H_{608}N_{122}O_{60})(C_2H_5NO_2)_2(C_{30}H_{45}N_9O_8)_{1.5}(C_{23}H_{30}N_4O_{10}S)_{27}(C_{37}H_{34}N_2O_{10}S_2)_{0.5}Na_{42}(H_2O)_{97}]$: C, 45.51; H, 6.58; N, 13.22; S, 3.44. Found: C, 45.81; H, 6.48; N, 12.60; S, 2.85. MALDI-TOF expected for $[\mathbf{6b}\cdot Na_2(H_2O)_{441}]^{2+}$: 17 138; Found: m/z = 17 138.

Complexation of Gd(III) by 1B4M-DTPA-pendant dendrimers (7)

The pendant 1B4M-DTPA chelates in **6** were used to complex Gd(III) by addition of $Gd(OAc)_3$. In brief, $Gd(OAc)_3$ (38 mg, 0.114 mmol) was added to **6a** (90 mg, 3.75 mmol) or to **6b** (90 mg, 3.75 mmol) in 0.3 M citrate buffer (50 mL) (pH 4.5). After incubation in the dark at 25°C for 18 hr under argon with constant stirring, the solution was subjected to an exhaustive membrane dialysis using Amicon® membranes having a 3,000 Da molecular weight cutoff. Dialysis was initially performed against 0.1 M NH_4OAc (pH 7.0) to aid in complete removal of uncomplexed Gd(III), followed by an exhaustive dialysis against H_2O. Lyophilization of the retentates provided the products as fluffy light-purple hygroscopic solids: 110 mg **7a** and 108 mg **7b**. The content of bound Gd(III) per molecule of dendrimer was determined by elemental analysis using inductively coupled plasma-atomic emission spectroscopy (ICP-AES). The composition of selected modified dendrimer products are shown in Table 1. Elemental analysis calculated for **7a** $[(C_{302}H_{608}N_{122}O_{60})(C_2H_5NO_2)_2(C_{29}H_{43}N_9O_8)_2(C_{23}H_{30}N_4O_{10}S)_{27}(C_{37}H_{34}N_2O_{10}S_2)_{0.75}(C_6H_7O_3)_{35}Gd_{23}Na_{20}(H_2O)_{265}]$: C, 37.31; H, 5.93; N, 8.96; S, 2.32; Gd, 9.20. Found: C, 37.70;

H, 5.47; N, 8.80; S, 1.88; Gd, 9.35. MALDI-TOF expected for [**7a**·Na$(H_2O)_{301}]^{2+}$: 19 046; Found: m/z = 19 046. Elemental analysis calculated for **7b** [$(C_{302}H_{608}N_{122}O_{60})$ $(C_2H_5NO_2)_2(C_{30}H_{45}N_9O_8)_{1.5}(C_{23}H_{30}N_4O_{10}S)_{27}$ $(C_{37}H_{34}N_2O_{10}S_2)_{0.5}$ $(C_6H_7O_3)_{15}Gd_{18}Na_{15}(H_2O)_{160}]$: C, 40.21; H, 6.05; N, 10.71; S, 2.78; Gd, 8.78. Found: C, 40.23; H, 5.64; N, 11.13; S, 2.11; Gd, 8.74. MALDI-TOF expected for [**7b**·$Na_2(H_2O)_{351}]^{2+}$: 18 032; Found: m/z = 18 033.

Relaxivity measurements

Solutions of compounds **7a** and **7b** (0.25–1.0 mM) in 1X PBS (300 μL volume) were prepared along with a corresponding set from the G4-1B4M$_{60}$-Gd$_{42}$[11] and Magnevist for comparison purposes. Measurements were obtained at ~22 °C using a 3-Tesla clinical scanner (Signa Excite, General Electric Medical System, Waukesha, WI) equipped with a rectangular single loop receiver coil (84 × 126 × 6 mm). Images of the solutions using an 8-echo 2D-spin echo (2D-SE) sequence were acquired with repetition times of 167, 300, 617, 1250, 2500 and 5000 ms at an echo time of 9.2 ms. T_1 and T_2 maps were calculated using the ImageJ MR Analysis plug-in (http://rsb.info.nih.gov/ij/plugins/mri-analysis.html). T_1 and T_2 relaxivities, r_1 and r_2, were determined from the slopes of the plot of relaxation rates, $R_1 = 1/T_1$ and $R_2 = 1/T_2$, vs [Gd].

Confocal fluorescence microscopy studies

M21 melanoma cells were grown at 37°C in the presence of 5% CO_2 in DMEM medium supplemented with 1% L-glutamine, and 5% FBS. For the confocal fluorescence microscopy experiments cells were plated in Lab-Tek chambered coverglasses (#155411, Nalge Nunc) at an appropriate dilution and allowed to attach overnight at 37°C prior to treatment. The mouse anti-human integrin $\alpha_v\beta_3$ specific monoclonal antibody LM609 (Chemicon MAB1976X, Alexa Fluor 488 conjugated) was used to demonstrate localization of the vitronectin receptor (integrin $\alpha_v\beta_3$ complex). In all experiments, LM609 was used at a concentration of 50 μg/mL. **6a** and **6b** were diluted into culture medium at 1.0 μM or 10 μM, while c(RGDfK)-Alexa Fluor 594 and c(RADfK)-Alexa Fluor 594 were diluted at 1.0 μM. Chambered cover glasses containing 60–80% confluent M21 cells were incubated for 2 or 2.5 hr at 37°C in the dark for **6a** and **6b**, while 30 min for the peptide-dye conjugates. After incubation, the solution was removed and slides were washed three times with PBS (pH = 7.4) and immediately fixed in 4% paraformaldehyde prepared in PBS (pH = 7.4) for 5 min at room temperature. Fluorescent mounting medium (S3023, DakoCytomation) was added to the individual chambers to stabilize the fluorophores before and during confocal microscopy.

Confocal images were acquired on a Zeiss LSM 510 NLO confocal system (Carl Zeiss, Thornwood, NJ, USA) mounted on a Zeiss Axiovert 200M inverted microscope and operating with a 30 mW argon laser tuned to 488 nm and a 1 mW HeNe laser tuned to 543 nm. Images were collected using a 63x Plan-Apochromat 1.4 NA oil immersion objective and a multi-track configuration where the Alexa Fluor 488 and Alexa Fluor 594 signal were sequentially collected with a BP 510/20 IR nm filter and BP 565–615 nm filters after excitation with 488 nm and 543 nm laser lines, respectively. In the sequential acquisitions for all two channels the Zeiss AIM software version 3.2 sp2 (Carl Zeiss GmbH, Heidelberg, Germany) was used. All confocal images were acquired with a frame size of 512 by 512 pixels averaged four times.

NIR optical imaging

NIR optical imaging was performed using the Maestro spectroscopic imaging unit (CRI, Waltham, MA, USA) using an excitation 590 nm band-pass filter and an emission 618-nm long-pass filter. Images were obtained at 10-nm intervals through the visible spectrum and spectra images of the AlexaFluor 594 and background autofluorescence were generated. These were unmixed to differentiate AlexaFluor 594 labeled tissue from background

autofluorescence, and were displayed. Immediately after *in vivo* NIR fluorescence imaging, mice were killed with CO_2 inhalation at 5 hr post-injection. The tumor and organs were harvested for *ex vivo* fluorescence imaging.

Radiosynthesis and characterization of ^{111}In(III)-7a and ^{111}In(III)-CHX-A''-c(RGDfK)

Caution: ^{111}In ($t_{1/2}$ = 63.31 hr) is a γ-emitting (E_γ=171.3 keV) radionuclide with associated Auger electron emission resulting from electron capture (EC) decay. Appropriate shielding and handling protocols should be in place when using this radionuclide. A 500 μCi aliquot of ^{111}In (Perkin Elmer, Wellesley, MA) in 0.05 N HCl was added to 0.1 mg (3.4 nmol) **7a** or ^{111}In(III)-CHX-A''-c(RGDfK) dissolved in 100 μL of 0.15M NH_4OAc (pH 7). The reaction mixture was incubated at 37 °C for 30 min. The ^{111}In- **7a** product was separated from uncomplexed ^{111}In by size-exclusion chromatography on a G3000SW column (Tosoh Biosciences) at 1 mL/min (isocratic 1X PBS pH 7.0). Conversely, ^{111}In(III)-CHX-A''- c (RGDfK) was purified by RP-HPLC using a Vydac Protein & Peptide C_{18} column equilibrated with 15 mM NH_4OAc (pH 7). A gradient of CH_3CN that increased from 0% to 100% for 40 min was employed. In both cases, a UV detector (Gilson 112 UV/Vis) and radiometric detector (γ-RAM, INUS Systems, Inc) were coupled to measure absorbance at 254 nm and radioactivity, respectively.

Biodistribution studies of ^{111}In(III)-7a and ^{111}In(III)-CHX-A''-c(RGDfK)

All procedures were performed in accordance with the National Institutes of Health guidelines on the use of animals in research and were approved by the Animal Care and Use Committee of the National Cancer Institute. All *in vivo* studies were performed with 4 to 6-week-old female athymic (nu/nu) mice (Charles River Laboratories, Wilmington, MA). The human melanoma cell line, M21, was grown in RPMI-1640 supplemented with 10% FetalPlex (Gemini Bioproducts, Woodland, CA), 1 mM NEAA, and 2 mM L-glutamine. All media and supplements were obtained from Quality Biologicals (Gaithersburg, MD) unless otherwise specified. Mice received s.c. injections in the right flank with 4×10^6 M21 melanoma cells in 0.2 mL of medium. Mice were used in studies when the tumor xenografts maximal diameter measured 0.4 to 0.6 cm. Mice (n = 3 per time point) received i.v. injections of ^{111}In(III)-**7a** (~10 μCi) or ^{111}In(III)-CHX-A''-c(RGDfK) and were sacrificed by exsanguination at the desired time points (1, 2, and 4 hr for ^{111}In(III)-**7a**; 1, 2, 6, 24, and 48 hr for ^{111}In(III)-CHX-A''-c(RGDfK)). The blood, tumor, and major organs were collected, wet-weighed, and counted in a γ-scintillation counter (1480 Wizard 3", PerkinElmer, Shelton, CT). The percent injected dose per gram (%ID/g) and SD were calculated.

RESULTS AND DISCUSSION

Dendrimers are a well-defined class of highly branched, synthetic polymers with a wide array of possible chemical structures and functional groups.[3,35] Their controlled structure and size attributes provide an attractive platform for development of reproducible chemistry for biomedical applications,[1–3] including development of imaging and MR contrast agents.[4]

Dendrimer-based Gd(III) macromolecular MR contrast agents have proven to have high relaxivities providing high resolution images.[4,8] In these studies, PAMAM G3 dendrimers were chosen as the scaffolding to carry multiple copies of chelators primarily due to size appropriateness (e.g., ~3 nm), established biological behaviors, and commercial availability permitting comparative studies.[10] Previously, PAMAM G3 dendrimers conjugated with chelated Gd(III) were reported to undergo rapid renal excretion while also being near exclusively retained in the blood vessels or urinary tracts with minimal extravasation.[10,36,37] Low-generation dendrimer-based agents including G2 (3 nm), G3 (5 nm) and G4 (6 nm) gadomers were quickly excreted primarily during the first pass via the kidney as determined

by biodistribution and excretion studies.[10,36,37] Although such smaller dendrimer-based MRI contrast agents are more quickly excreted by the kidneys, they are also able to visualize vascular structures better than Gd-DTPA due to less extravasation.[10,36] For targeting integrin $\alpha_v\beta_3$, the optimal generation dendrimer would allow for extravasation within leaky tumor blood vessels but would not extravasate in normal vasculature. Intermediate-generation agents including G5 (7 nm) and G6 (9 nm) gadomers were more slowly excreted via the kidney due to a prolonged blood pool retention; however, these generations also begin to show signs of partial hepatobiliary excretion.[10,37] Almost exclusively hepatobiliary excretion was observed for G7 (11 nm) and G8 (13 nm), while anything larger becomes entrapped by the reticuloendothelial system (liver and spleen).[10] Taking all of these factors into consideration, we chose G3 as a scaffold for the following reasons: (1) to offset the slightly hydrophobic peptide and dye modifications that add to the overall macromolecular size and may have further encouraged hepatobiliary excretion and (2) to take advantage of the decreased extravasation with respect to a low-molecular weight peptide targeting the integrin. It is quite possible, however, that better *in vivo* targeting may have been realized through selection of a larger generation (e.g. G5) having slower renal clearance, thereby giving the targeted dendrimeric agent more time to bind integrin $\alpha_v\beta_3$ expressed on the tumor and associated vasculature. It is likely, however, that increased hepatic uptake would limit the efficacy of this approach. Furthermore, better *in vivo* results may have also been realized through the attachment of more than an average of two cyclic RGD peptides per G3 scaffold to increase multivalency effects of integrin binding; however, attachment of clusters of peptides similar to the approach followed by Boturyn and coworkers may offer greater advantages by allowing control over the distance between multiple cyclic peptides.[34]

The synthetic strategies employed here were intended to provide a general synthesis for dendrimer-based contrast agents bearing peptides or other receptor-targeted moieties. Use of the isothiocyanate (chelating agent) and *N*-hydroxysuccinimidyl active ester (NIR dye) groups were justified by established usage, reaction efficiencies, and the *in vivo* stability of resultant thiourea and amide groups. Selection of an orthogonal aminooxy/aldehyde strategy for peptide-dendrimer conjugation fulfilled a special need to introduce a cyclic peptide containing a carboxylic acid.

The peptide-to-dendrimer product ratio potentially might be controlled by making the peptide aldehyde the limiting reagent; however, in these studies the controlling factor was chosen to be the amount of *N*-hydroxysuccinimidyl ester of *N*-(*tert*-butoxycarbonyl)-*O*-(carboxymethyl) hydroxylamine (**1**) reacted with the dendrimer. The peptide-to-dendrimer product ratio can be estimated by ^{1}H NMR peak integration of dendrimer protons versus the unique BOC (CH_3) or methylene (CH_2) protons of the aminooxy moiety. However, this characterization technique must be approached with caution given the broad nature of dendrimer proton peaks. Additionally, one must assume that the peptide aldehyde was reacted in sufficient amount to consume all of the aminooxy residues. A product target of an average number of 2 peptide moieties and 1 dye molecule per dendrimer was chosen. However, due to analytical difficulties, *e.g.*, broad NMR peaks, broad MALDI-TOF mass peaks, salts and H_2O complicating combustion analyses, in reality characterization for such dendrimer based poly-component materials became quite challenging to establish with complete certainty absolutes (*vida infra*).

Thus, characterization of these macromolecular compounds is a formidable challenge. The ^{1}H NMR spectra of dendrimers were characterized by very broad signals (see Supporting Information). Thus, as noted above integration provides only estimated values. Matrix-assisted laser desorption ionization time-of-flight (MALDI-TOF) mass spectrometry was also of limited value due to broad signals (see Supporting Information). Elemental analyses making use of the sulfur component was also used for the determination of the number of chelates on

the dendrimer scaffold. This data indicated that ~27 chelates were covalently attached to the surface of dendrimer, corresponding to 93% saturation of a total of ~29 remaining amino groups (assuming conjugation of 2 peptides and 1 dye molecule per dendrimer).

Aminooxy functionalization of dendrimer

The ^{1}H NMR spectrum (see Supporting Information) shows conjugation of **1** to G3 PAMAM dendrimer. An inability to successfully purify the unconjugated low-molecular weight species from the conjugate (**2**) is explained by the hydrophobic nature of **1** as is observed by its low solubility in water. The literature-reported ^{1}H NMR ppm values for the BOC and the methylene protons of the **1** in DMSO(d_6) are δ 1.42 (s, 9H, CH_3) and δ 4.83 (s, 2H, CH_2O), respectively while the values for the acid are δ 1.40 (s, 9H, CH_3) δ 4.26 (s, 2H, CH_2), respectively.[33] The spectrum of **2** contains two different peaks in the region where BOC (CH_3) protons are observed at δ 1.21 and δ 1.42. The "BOC" peak at δ 1.42 is assigned to the starting material **1**, while the peak at δ 1.21 is assigned to the desired G3-dendrimer conjugate product (**2**). Interactions between the BOC protons and G3 protons may be responsible for an apparent upfield shift relative to the BOC protons of unconjugated **1**. The third "BOC" peak at δ 1.7 can be assigned to a small amount of hydrolysis product of **1**, shifted downfield due to the presence of the basic amines of the dendrimer.

Further insight is obtained from the methylene proton signals at δ 4.18 and δ 4.37. The δ 4.37 signal agrees with the literature-reported value for **1** in D_2O while we assigned the δ 4.18 as the methylene protons for the conjugate **2** product. A third methylene peak for the acid hydrolysis product of **1** may fall under the prominent water peak and would not have been obvious due to its abundance. Both conjugated and unconjugated forms of **1** are responsible for the presence of two sets of peaks for the methyl and methylene peaks.

The ^{1}H NMR spectrum shows successful and complete acid deprotection of the BOC evident by complete disappearance of CH_3 peaks in the δ 1–2 range. Additionally, a single methylene signal at δ 4.20 indicates that purification at this step successfully removed unconjugated aminooxy species (**1**).

Oxime-ligation of c(RXDfK)-peptide aldehyde to aminooxy-modified dendrimers (4)

Successful formation of the respective peptide aldehydes by periodate oxidation was confirmed by high-resolution electrospray mass spectrometry. The ^{1}H NMR spectrum confirms successful oxime ligation of the c(RGDfK) peptide aldehyde to the aminooxy-pendant G3 PAMAM dendrimer. In contrast to the clean methylene (CH_2) singlet observed in **3**, numerous new signals of relatively low intensity are apparent for **4** that closely match the ^{1}H spectrum of c(RGDfK(S)) under similar conditions. The aromatic protons (phenylalanine residue (δ 7–8)) are easily identified, while other residues are obscured by the core dendrimer region (δ 2–4). Similar results were observed for the c(RADfK) peptide-G3 dendrimer conjugate.

Sequential conjugation of Alexa Fluor 594 and 1B4M-DTPA to c(RXDfK)-modified dendrimers (6)

Modification of the dendrimer-peptide conjugates with metal chelators (1B4M-DTPA) and dye (Alexa Fluor 594) was monitored by MALDI mass spectrometry, defined by elemental analyses, with the purity being assessed by size-exclusion HPLC. HPLC chromatograms of both cRGD- and cRAD-containing chelate-dye-dendrimer constructs, **6a** and **6b**, respectively, (monitoring UV signal at 254 nm) unsurprisingly showed multiple high-molecular weight species, consistent with speciation and/or a distribution of products (see Supporting Information).

Although a 2:1 molar ratio of 2-(4-isothiocyanatobenzyl)-6-methyl-diethylenetriamine pentaacetic acid (1B4M-DTPA) to surface primary amines of the dendrimer was used in all syntheses, the average number of 1B4M-DTPA units conjugated per dendrimer macromolecule, ~27, falls short of the theoretical maximum value (29) for these dendrimers assuming an average of two units of the peptide and one molecule of the dye. This observation is consistent with previously reported data.[16] Saturation is difficult to achieve or control, even in the case of relatively small dendrimers. However, full saturation is also not always desirable. Retention of an available primary amine provides a site for introduction of another moiety such as an optical dye molecule. In this case, limitations to saturation most probably reside with the chelating agent and reaction conditions. The efficiency of aqueous isothiocyanate conjugation chemistry is known to compete with disproportionation and decomposition reactions at the relevant pH and temperature. Additionally, limitations imposed by steric crowding by the conjugation of the chelating agent and/or lack of access to remaining surface primary amines are important factors. Research is currently underway to refine organic phase chemistry for dendrimer-chelate conjugation.[11]

The fluorescence quantum yields of the dye following conjugation as determined by fluorimetry were lower than anticipated (Φ_F = 0.30 for **6a**; Φ_F = 0.37 for **6b**) (Table 1). This is possibly due to chemically-induced bleaching of the dye by impurities and/or by-products resulting from the isothiocyanate mediated chelate conjugation immediately following dye conjugation. This unfortunate result reinforces that conjugation of dyes should be incorporated into synthetic procedures as late as possible. Even following the conjugation with excess chelate, a few remaining unreacted terminal amines are more likely present for dye conjugation.

Complexation of Gd(III) by 1B4M-DTPA-pendant dendrimers (7)

Modification of the dendrimer-peptide-chelate-dye constructs by Gd(III) complexation was again monitored by MALDI mass spectrometry and defined by elemental analyses. Purity was assessed by size-exclusion HPLC. HPLC chromatograms of both **7a** and **7b** (monitoring UV signal at 254 and 280 nm) continued to show multiple high-molecular weight species, consistent with speciation and/or a distribution of products as expected with the distribution of products observed in the previous step (see Supporting Information).

Molar relaxivity measurements were performed on a side-by-side comparison with Magnevist™ and a simple G4 Gd(III)-1B4M-DTPA compound[11] using a 3-Tesla clinical scanner. A r_1 relaxivity of 8.78 $mM^{-1}s^{-1}$ was obtained for **7a**, while a r_1 relaxivity of 10.09 $mM^{-1}s^{-1}$ was obtained for **7b** consistent with the generation size (Table 1).

Confocal fluorescence microscopy

Confocal fluorescence microscopy was performed on the peptide-dye conjugates, and on the peptide-functionalized dendrimers with and without complexed Gd(III) (Figure 3 and 4). Confocal fluorescence microscopy imaging demonstrated cell surface binding and internalization of c(RGDfK)-AlexaFluor 594 (Figure 3A) and c(RGDfK)-functionalized dendrimer **6a** (Figure 3C, Figure 4A) but not c(RADfK)-AlexaFluor 594 (Figure 3B) and c (RADfK)-functionalized **6b** (Figure 3D, Figure 4B) to cultured M21 cells. The observed internalization of c(RGDfK)-Alexa Fluor 594 is consistent with reported data for a c(RGDfK)-carboxyfluorescein conjugate.[38] Binding of LM609, an antibody against $\alpha_v\beta_3$ integrin,[39] was also observed, and colocalization with **6a** was demonstrated (Figure 3C, Figure 4A). Selective binding of **6a** over **6b** was demonstrated by cell surface binding and internalization of **6a**, but not **6b** to cultured M21 cells (Figure 3C, 4A, 4B). However, the corresponding Gd(III)-complexed products, **7a** and **7b**, did not show the same level of selectivity (Figure 4C, 4D), possibly due to non-specific cell surface binding and/or internalization that may have resulted from the increased hydrophobicity and aggregation of the complex due to charge neutralization.

Another reported PAMAM dendrimer-based nanodevice bearing the c(RGDfK) peptide motif demonstrated selective $\alpha_v\beta_3$ binding over an analogous nanodevice lacking any peptide functionalization at all.[40] Our approach has the advantage that **6a** and **6b**, differing only in a single methyl group, are more similar in terms of size and hydrophilicity than two nanodevices with and without peptides.

NIR optical imaging

NIR optical imaging provided surprisingly little useful information during *in vivo* imaging with anaesthetized mice using both **7a** and **7b**; as a result, *ex vivo* imaging of the tumor and major organs were performed at 5 hr post-injection to improve signal acquisition. While uptake in kidneys is evident for both agents, little other information was obtained. This may be a result of the low fluorescence quantum yields of both final products (*vide infra*).

Radiosynthesis and characterization of 7a and ^{111}In(III)-CHX-A''-c(RGDfK)

Incorporation of ^{111}In into the chelate-peptide conjugate was performed using previously described conditions.[41] Conditions similar to those used for radiolabeling antibodies were applied to these complex macromolecular constructs in anticipation that an adequate number of empty chelates would be available. Size-exclusion radiochromatography demonstrated successful radiolabeling of the modified dendrimer with ^{111}In. Radiochemical yields (unoptimized) of 33% (5 μCi/μg) were obtained. These results are of extreme importance as they provide a means for accurate tracer studies including both tissue distribution and imaging by either single photon emission computed tomography (SPECT) imaging or positron emission tomography (PET) imaging *via* ^{86}Y.

Biodistribution studies of 7a and ^{111}In(III)-CHX-A''-c(RGDfK)

The biodistributions of ^{111}In-labeled modified dendrimer and the direct peptide-chelate conjugate were evaluated in M21 tumor-bearing mice (Figure 5), an established model for $\alpha_v\beta_3$ expression.[42] The major organs of uptake for the dendrimer were the kidneys, liver, and spleen. Data obtained at 1, 2, and 4 hr post-injection suggest that the kidneys have the highest uptake at each time point, followed by liver, and then spleen. The peak % injected dose per gram (%ID/g) values were 65.95 ± 5.87 for kidneys, 48.73 ± 4.71 for liver, and 13.58 ± 2.17 for spleen at 2 hr. The %ID/g values for the M21 tumor xenograft were 0.91 ± 0.46, 1.25 ± 0.51, and 0.76 ± 0.17 at 1, 2, and 4 hr, respectively. The tumor:blood ratio peaked at 2 hr (3.30 ± .03).

The biodistribution of ^{111}In(III)-CHX-A''-c(RGDfK) was typical of that for small peptide-chelate conjugates and reveals very rapid blood clearance and much lower retention in kidneys, liver, and spleen relative to the peptide-dendrimer conjugate. The organ with highest uptake was the ovaries, but moderate hepatobiliary, intestinal, and renal uptake and clearance were also evident. It is of particular importance to note the difference in the Y-axis scales between the two graphs.

CONCLUSIONS

The synthesis, characterization, and biological evaluation of PAMAM dendrimers with chemoselectively-ligated RGD- or RAD-cyclopeptides have been presented. These complex macromolecular constructs were synthesized in a rational, step-wise manner taking advantage of orthogonal aminooxy/aldehyde coupling chemistry for peptide conjugation and by using standard succinimidyl ester and isothiocyanate chemistry for dye and chelate conjugation, respectively. In this step-wise preparation of the multimodal macromolecular imaging agent, conjugation of the optical dye would be best suited near the end of the assembly to avoid photobleaching.

In vitro studies have demonstrated the capability of this macromolecular construct as a MR contrast agent and as an optical agent. Through fluorescence microscopy, we have demonstrated selectivity of the cRGD-containing dendrimer (**6a**) over the control negative cRAD-containing dendrimer, consistent with the corresponding peptide-dye conjugates, to cultured M21 cells that are known to highly express the $\alpha_v\beta_3$ integrin. However, *in vivo* studies by optical fluorescence imaging and biodistribution studies through the use of ^{111}In-radiolabeling have failed to demonstrate appreciable tumor uptake indicating either an inability of the agent to go extravascular into the tumor or a poor choice of the target or targeting moiety.

Supplementary Material

Refer to Web version on PubMed Central for supplementary material.

ACKNOWLEDGMENTS

This research was supported by the Intramural Research Program of the NIH, National Cancer Institute, Center for Cancer Research. This project has been funded in part with federal funds from the National Cancer Institute, National Institutes of Health, under contract N01-CO-12400.

We would also like to thank Dr. Steven K. Libutti for the helpful discussions on angiogenesis and the M21 tumor model.

REFERENCES

1. Boas U, Heegaard RMH. Dendrimers in drug research. Chem. Soc. Rev 2004;33:43–63. [PubMed: 14737508]
2. Boas, U.; Christensen, JB.; Heegaard, PMH., editors. Dendrimers in Medicine and Biotechnology. Cambridge: RSC Publishing; 2006.
3. Lee CC, MacKay JA, Frechet JMJ, Szoka FC. Designing dendrimers for biological applications. Nat. Biotech 2005;23:1517–1526.
4. Wiener, E.; Narayanan, Venkatraj. Magnetic resonance imaging contrast agents: theory, and the role of dendrimers. In: Newkome, GR., editor. Advances in Dendritic Macromolecules. New York: Elsevier Science Ltd.; 2002. p. 129-247.
5. Wiener EC, Brechbiel MW, Brothers H, Magin RL, Gansow OA, Tomalia DA, Lauterbur PC. Dendrimer-based metal chelates: a new class of magnetic resonance imaging contrast agents. Magn. Reson. Med 1994;31:1–8. [PubMed: 8121264]
6. Knopp MV, Tengg-Kobligk H, Choyke PL. Functional magnetic resonance imaging in oncology for diagnosis and therapy monitoring. Molec. Cancer Ther 2003;2:419–426. [PubMed: 12700286]
7. Yordanov AT, Kobayashi H, English SJ, Reijnders K, Milenic DE, Krishna MC, Mitchell JB, Brechbiel MW. Gadolinium-labeled dendrimers as biometric nanoprobes to detect vascular permeability. J. Mater. Chem 2003;13:1523–1525.
8. Venditto VJ, Regino CAS, Brechbiel MW. PAMAM dendrimer based macromolecules as improved contrast agents. Molecular Pharm 2005;2:302–311.
9. Yordanov AT, Kobayashi H, English SJ, Reijnders K, Milenic DE, Krishna MC, Mitchell JA, Brechbiel MW. Gadolinium-labeled dendrimers as biometric nanoprobes to detect vascular permeability. J. Mater. Chem 2003;13:1523–1525.
10. Kobayashi H, Brechbiel MW. Nano-sized MRI contrast agents with dendrimer cores. Adv Drug Deliv. Rev 2005;57:2271–2286. [PubMed: 16290152]
11. Xu H, Regino CAS, Bernardo M, Koyama Y, Kobayashi H, Choyke PL, Brechbiel MW. Towards improved syntheses of dendrimer-based MR contrast agents: new bifunctional DTPA ligands and non-aqueous conjugation chemistry. J. Med. Chem 2007;50:3185–3193. [PubMed: 17552504]
12. Kobayashi H, Sato N, Saga T, Nakamoto Y, Ishimori T, Toyama S, Togashi K, Konishi J, Brechbiel MW. Monoclonal antibody-dendrimer conjugates enable radiolabeling of antibody with markedly high specific activity with minimal loss of immunoreactivity. Eur. J. Nucl. Med 2000;27:1334–1339. [PubMed: 11007515]

13. Konda SD, Aref M, Wang S, Brechbiel MW, Wiener EC. Specific targeting of folate-dendrimer MRI contrast agents to the high affinity folate receptor expressed in ovarian tumor xenografts. MAGMA 2001;12:104–113. [PubMed: 11390265]

14. Shukla R, Thomas TP, Peters J, Kotlyar A, Myc A, Baker JR. Tumor angiogenic vasculature targeting with PAMAM dendrimer-RGD conjugates. Chem. Comm 2005:5739–5741. [PubMed: 16307130]

15. Langereis S, Dirksen A, de Waal BFM, van Genderen MHP, de Lussanet QG, Hackeng TM, Meijer EW. Solid-phase synthesis of a cyclic NGR-functionalized Gd(III)DTPA complex. Eur. J. Org. Chem 2005;12:2534–2538.

16. Talanov VS, Regino CAS, Kobayashi H, Bernardo M, Choyke PL, Brechbiel MW. Dendrimer-based nanoprobe for dual modality magnetic resonance and fluorescence imaging. Nano. Lett 2006;6:1459–1463. [PubMed: 16834429]

17. De S, Razorenova O, McCabe NP, O'Toole T, Qin J, Byzova TV. VEGF-integrin interplay controls tumor growth and vascularization. Proc. Natl. Acad. Sci. U.S.A 2005;102:7589–7594. [PubMed: 15897451]

18. McQuade P, Knight LC. Radiopharmaceuticals for targeting the angiogenesis marker alpha-v-beta-3. Q. J. Nucl. Med 2003;47:209–220. [PubMed: 12897712]

19. Conforti G, Dominguez-Jimenez C, Zanetti A, Gimbrone MA Jr, Cremona O, Marchisio PC, Dejana E. Human endothelial cells express integrin receptors on the luminal aspect of their membrane. Blood 1992;80:437–446. [PubMed: 1627801]

20. Zitzmann S, Ehemann V, Schwab M. Arginine-glycine-aspartic acid (RGD)-peptide binds to both tumor and tumor-endothelial cells in vivo. Cancer Res 2002;62:5139–5143. [PubMed: 12234975]

21. Regino CAS, Boswell CA, Milenic DE, Wong KJ, Shaw C, Choyke PL, Brechbiel MW. Novel synthetic peptide scaffolds for multivalent-targeted imaging agents. J. Nucl. Med 2006;47

22. Mammen M, Choi S-K, Whitesides GM. Polyvalent interactions in biological systems: Implications for design and use of multivalent ligands and inhibitors. Angew Chem Int. Ed 1998;37:2754–2794.

23. Wester HJ, Kessler H. Molecular targeting with peptides or peptide-polymer conjugates: Just a question of size? J. Nucl. Med 2005;46:1940–1945. [PubMed: 16330555]

24. Line BR, Mitra A, Nan A, Ghandehari H. Targeting tumor angiogenesis: comparison of peptide and polymer-peptide conjugates. J. Nucl. Med 2005;46:1552–1560. [PubMed: 16157540]

25. Mitra A, Nan A, Papadimitriou JC, Ghandehari H, Line BR. Polymer-peptide conjugates for angiogenesis targeted tumor radiotherapy. Nucl. Med. Biol 2006;33:43–52. [PubMed: 16459258]

26. Ellegala DB, Leong-Poi H, Carpenter JE, Klibanov AL, Kaul S, Shaffrey ME, Sklenar J, Lindner JR. Imaging tumor angiogenesis with contrast ultrasound and microbubbles targeted to alpha-v-beta-3. Circulation 2003;108:336–341. [PubMed: 12835208]

27. Wu H, Beuerlein G, Nie Y, Smith H, Lee BA, Hensler M, Huse WD, Watkins JD. Stepwise in vitro affinity maturation of Vitaxin, an alpha-v-beta-3-specific humanized mAb. Proc. Natl. Acad. Sci. U.S.A 1998;95:6037–6042. [PubMed: 9600913]

28. Gottschalk KE, Kessler H. The structures of integrins and integrin-ligand complexes: Implications for drug design and signal transduction. Angew Chem. Int. Ed 2002;41:3767–3774.

29. Cremer GA, Bureaud N, Lelievre D, Piller V, Piller F, Delmas A. Synthesis of branched oxime-linked peptide mimetics of the MUC1 containing a universal T-helper epitope. Chem. Eur. J 2004;10:6353–6360.

30. Geoghegan KF, Stroh JG. Site-directed conjugation of nonpeptide groups to peptides and proteins via periodate oxidation of a 2-amino alcohol. Application to modification at *N*-terminal serine. Bioconj. Chem 1992;3:138–146.

31. Brechbiel MW, Beitzel PM, Gansow OA. Purification of *p*-nitrobenzyl C-functionalized diethylenetriamine pentaacetic acids for clinical applications using anion-exchange chromatography. J. Chromatograph. A 1997;771:63–69.

32. Clifford T, Boswell CA, Biddlecombe GB, Lewis JS, Brechbiel MW. Small animal PET/CT imaging using ^{86}Y-CHX-A"-octreotide: Validation of a novel CHX-A" derivative suitable for peptide conjugation. J. Med. Chem 2006;49:4297–4304. [PubMed: 16821789]

33. Ide H, Akamatsu K, Kimura Y, Michiue K, Makino K, Asaeda A, Takamori Y, Kubo K. Synthesis and damage specificity of a novel probe for the detection of abasic sites in DNA. Biochemistry 1993;32:8276–8283. [PubMed: 8347625]

34. Boturyn D, Coll JL, Garanger E, Favrot MC, Dumy P. Template assembled cyclopeptides as multimeric system for integrin targeting and endocytosis. J. Am. Chem. Soc 2004;126:5730–5739. [PubMed: 15125666]

35. Tomalia DA, Baker H, Dewald J, Hall M, Kallos G, Martin S, Roeck J, Ryder J, Smith P. A new class of polymers: starburst-dendritic macromolecules. Polymer J 1985;17:117–132.

36. Kobayashi H, Kawamoto S, Jo SK, Bryant J, Brechbiel MW, Star RA. Macromolecular MRI contrast agents with small dendrimers: pharmacokinetic differences between sizes and cores. Bioconj. Chem 2003;14:388–394.

37. Kobayashi H, Sato N, Hiraga A, Saga T, Nakamoto Y, Ueda H, Konishi J, Togashi K, Brechbiel MW. 3D-Micro-MR angiography of mice using macromolecular MR contrast agents with polyamidoamine dendrimer core with reference to their pharmacokinetic properties. Magn. Reson. Med 2001;45:454–460. [PubMed: 11241704]

38. Castel S, Pagan R, Mitjans F, Piulats J, Goodman S, Jonczyk A, Huber F, Vilaro S, Reina M. RGD Peptides and monoclonal antibodies, antagonists of $\alpha_v\beta_3$-integrin, enter the cells by independent endocytic pathways. Laboratory Investigation 2001;81:1615–1626. [PubMed: 11742032]

39. Cheresh DA, Spiro RC. Biosynthetic and functional properties of an Arg-Gly-Asp-directed receptor involved in human melanoma cell attachment to vitronectin, fibrinogen, and von Willebrand factor. J. Biol. Chem 1987;262:17703–17711. [PubMed: 2447074]

40. Lesniak WG, Kariapper MST, Nair BM, Tan W, Hutson A, Balogh LP, Khan MK. Synthesis and characterization of PAMAM dendrimer-based multifunctional nanodevices for targeting αvβ3 integrins. Bioconj. Chem 2007;18:1148–1154.

41. Boswell CA, Clifford T, Biddlecombe G, Lewis JS, Brechbiel MW. A novel CHX-A" bifunctional chelator for *N*-terminal modification: Synthesis, characterization, and validation via Y-86 microPET/CT of somatostatin-positive tumors. J. Nucl. Med 2006;47

42. Petitclerc E, Stromblad S, von Schalscha TL, Mitjans F, Piulats J, Montgomery AMP, Cheresh DA, Brooks PC. Integrin alpha-v-beta-3 promotes M21 melanoma growth in human skin by regulating tumor cell survival. Cancer Res 1999;59:2724–2730. [PubMed: 10363998]

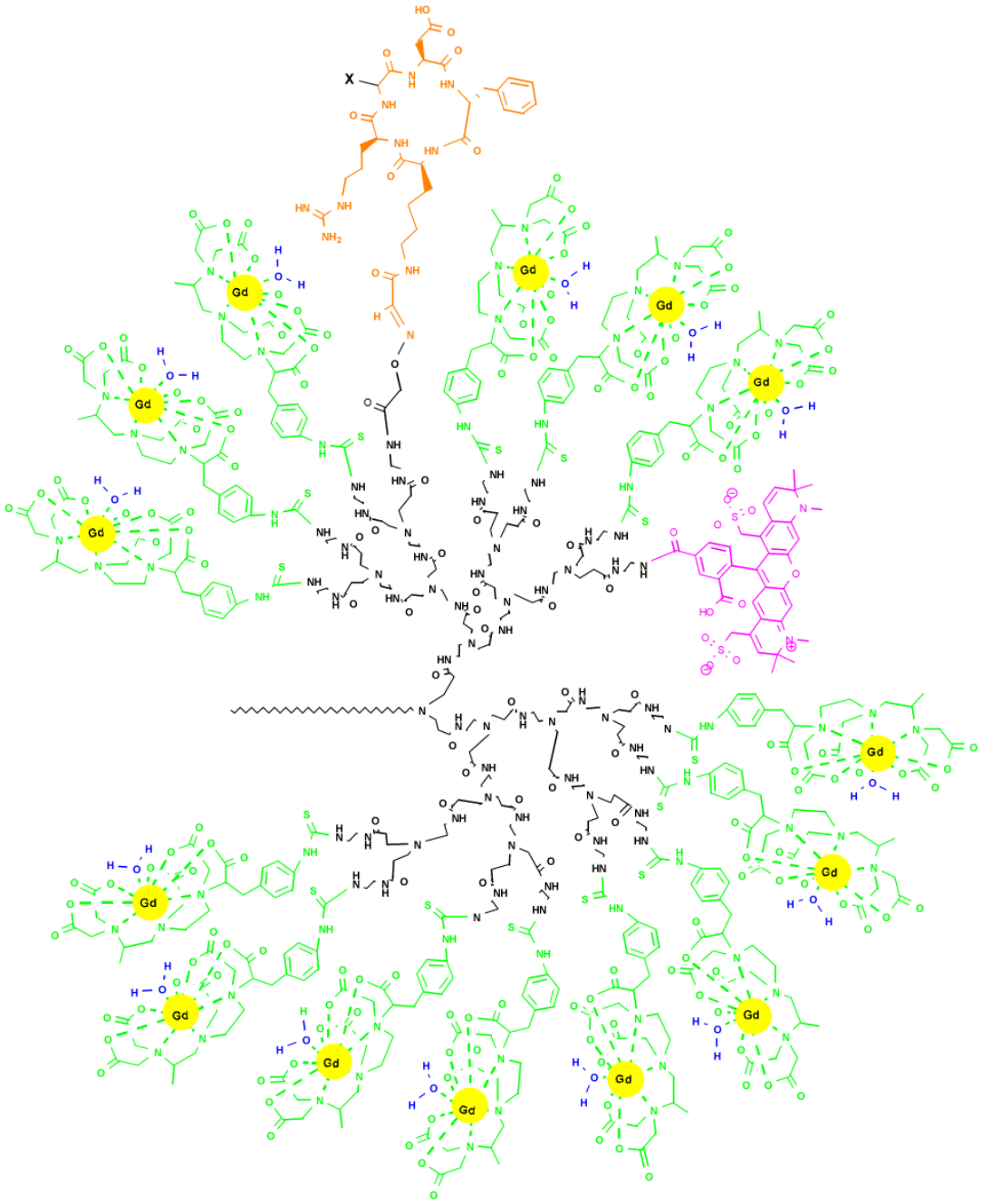

Figure 1.

Structural representation (half-section) of modified PAMAM dendrimer **7**. The PAMAM dendrimer core appears in black, the oxime-ligated $\alpha_v\beta_3$-targeting peptide, c(RGDfK), in orange, the 1B4M chelating agent in green, complexed Gd(III) as yellow spheres, and coordinating H_2O is blue.

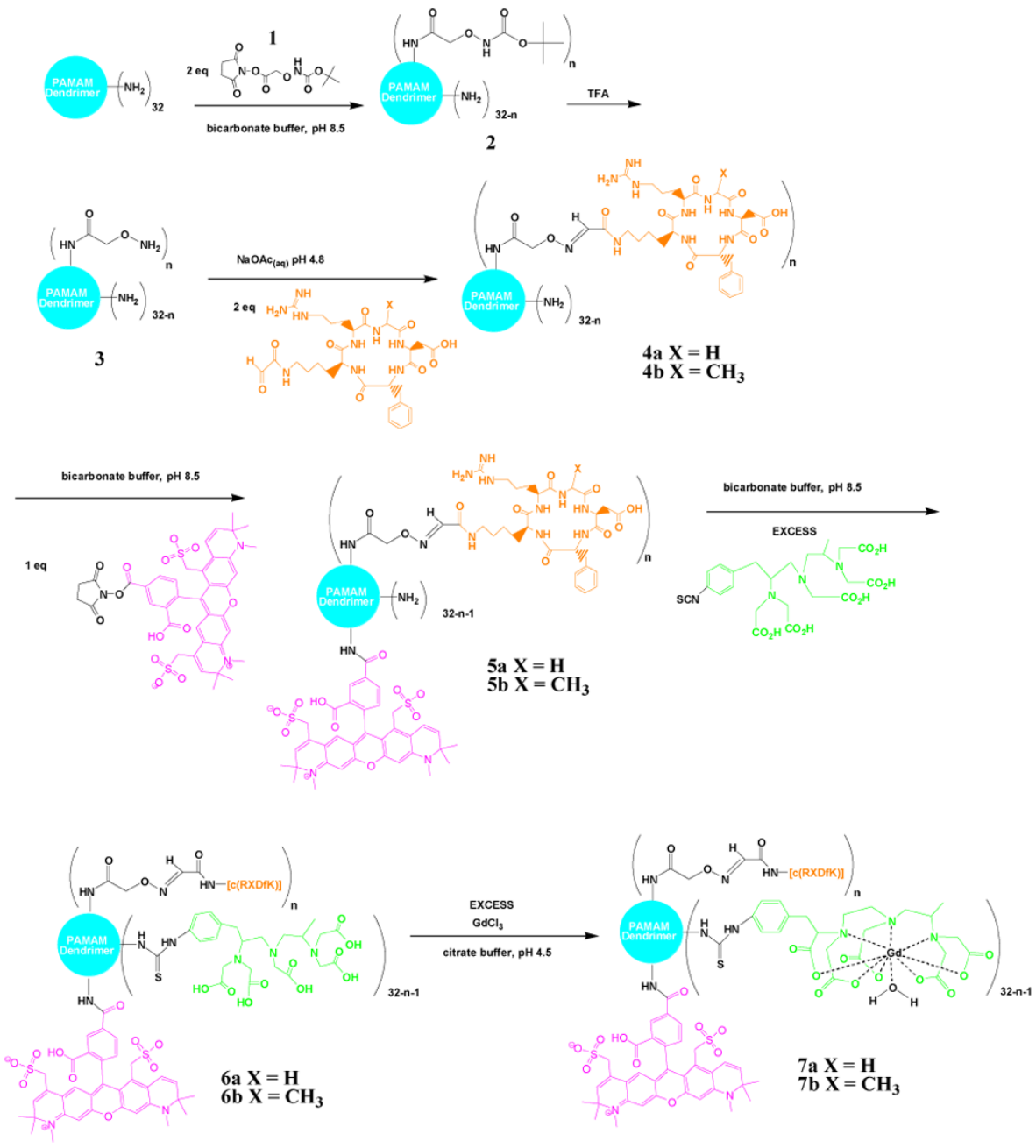

Figure 2.
General schematic representation of the stepwise modification of PAMAM dendrimers with cyclic-RGD-peptides, conjugation of Alexa Fluor 594 dye, saturation of remaining terminal amines with 1B4M, and chelation of Gd(III).

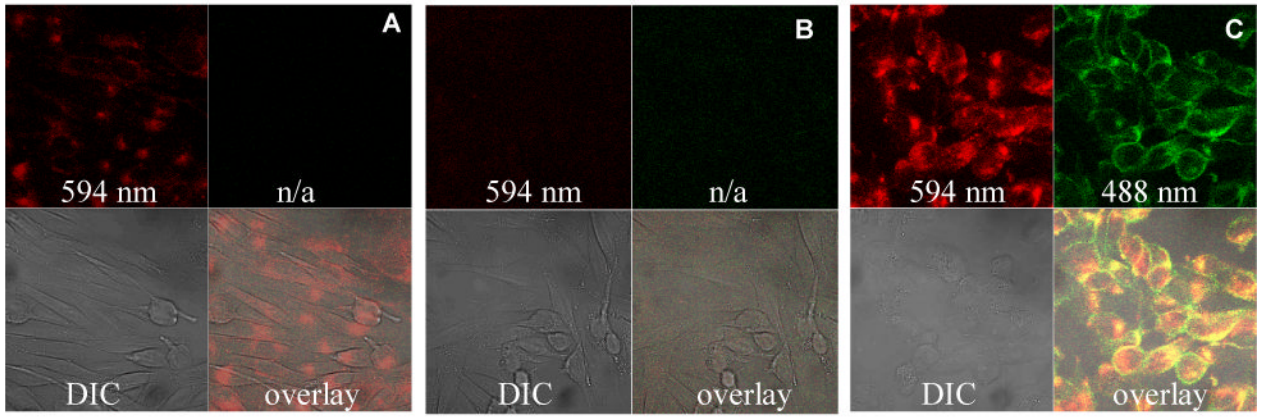

Figure 3.

Fluorescence confocal images of M21 cells incubated for 30 min (peptides, (A–B)) or 150 min (**6a**, (C)) in the absence (A–B) or presence (C) of LM609-Alexa Fluor 488 (anti-$\alpha_v\beta_3$ mAb) and (A) 1 μM c(RGDfK)-Alexa Fluor 594, (B) 1 μM c(RADfK)-Alexa Fluor 594, or (C) 1 μM **6a**. Each image displays Alexa Fluor 594 fluorescence represented in red (top left), the differential interference contrast (DIC) image (bottom left), and the overlay (bottom right). In image (C), Alexa Fluor 488 fluorescence is represented in green (top right), and yellow indicates co-localization.

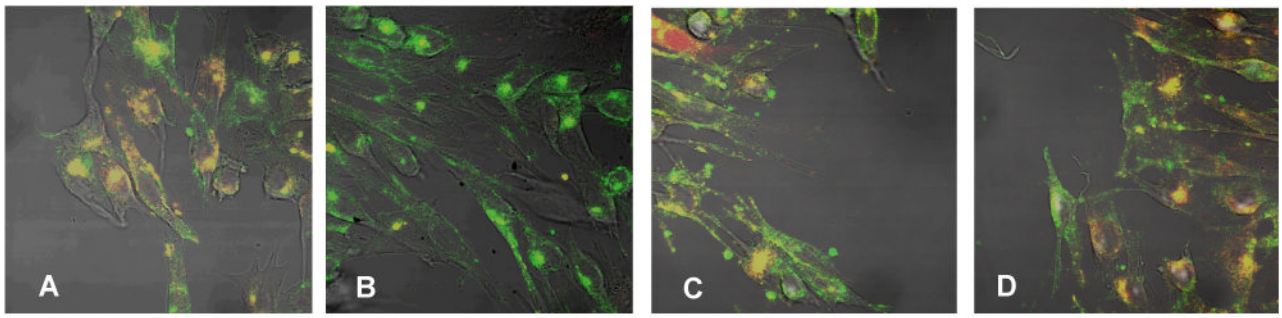

Figure 4.

Fluorescence microscopy overlay images of M21 cells incubated for 120 min in the presence of 50 μg LM609-ALexa Fluor 488 (anti-$\alpha_v\beta_3$ mAb) in (A) 10 μM **6a**, (B) 10 μM **6b**, (C) 10 μM **7a**, and (D) 10 μM **7b**. Alexa Fluor 488 conjugate is unmixed in green, Alexa Fluor 594 conjugates appear as red, and yellow indicates co-localization.

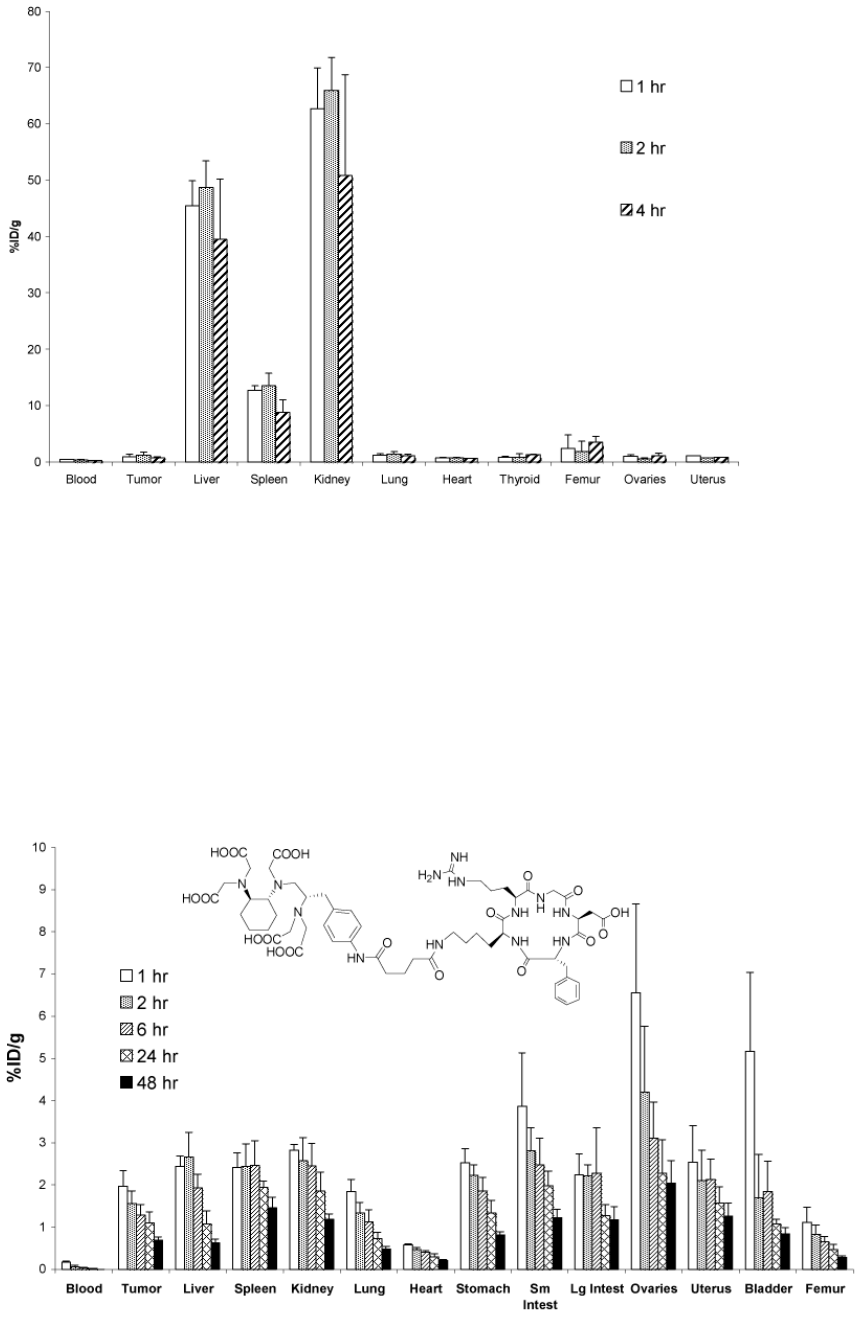

Figure 5.
Biodistributions of ^{111}In-**7a** (top) and ^{111}In-CHX-A''-c(RGDfK) (bottom) following i.v. injection in athymic mice bearing s.c. M21 melanoma tumors.

Table 1

Composition and characterization of the dendrimer-based nanomaterials.

Compound	# peptide units[a]	# dye units[a]	# 1B4M units[a]	# Gd^{3+a}	Φ(1X PBS)[b]	r_1,[b] $mM^{-1}s^{-1}$	r_2,[b] $mM^{-1}s^{-1}$
6a	2.6	0.75	27	-	0.30 ± 0.15	-	-
6b	1.5	0.5	27	-	0.37 ± 0.06	-	-
7a	2	0.75	27	23	0.32 ± 0.12	8.78 ± 0.22	17.70 ± 0.48
7b	1.5	0.5	27	18	0.31 ± 0.09	10.09 ± 0.12	23.84 + 0.51
Alexa Fluor 594	-	-	-	-	0.66[c]		

[a] Reported values are the average values as calculated from within 0.6% of the elemental analyses (C, H, N, S, and Gd) results which can be ± 0.5 of the mean value of the reported # of peptide, ± 0.25 of the mean value of the reported # of dye, ± 2 of the mean value of the reported # of 1B4M units, and ± 1 of the mean value of the reported # of Gd.

[b] Reported errors are standard errors.

[c] Reported relative quantum yield of Alexa Fluor 594 succinimidyl ester in 50 mM potassium phosphate, 150 mM NaCl pH 7.2 at 22 °C (Invitrogen).